Check for updates

Structurally diverse diterpenoid alkaloids from the lateral roots of *Aconitum carmichaelii* Debx. and their anti-tumor activities based on *in vitro* systematic evaluation and network pharmacology analysis†

Yang Yu, [ab] Shifei Wu, [a] Jianqing Zhang, [a] Jiayuan Li, [a] Changliang Yao, [a] Wenyong Wu, [ac] Yingying Wang, [ac] Hongjian Ji, [ac] Wenlong Wei, [a] Min Gao, [ab] Yun Li, [ad] Shuai Yao, [a] Yong Huang, [a] Qirui Bi, [a] Hua Qu [ac] and De-an Guo [ID] *[ab]

Thirty-seven diterpenoid alkaloids (DAs) with diverse structures were isolated and identified from the lateral roots of *Aconitum carmichaelii* Debx., comprising eight C_{20}-DAs and twenty-nine C_{19}-DAs. Besides the 31 known DAs identified by comparing the ^{1}H NMR and ^{13}C NMR data with those reported in the literature, the structures of four new compounds (**1**, **14**, **17**, and **25**), and two other compounds (**26** and **37**) which were reported to be synthesized previously, were also elucidated based on the comprehensive analysis of their HR-ESI-MS, 1D and 2D NMR spectra, including ^{1}H–^{1}H COSY, HSQC and HMBC and NOESY/ROESY. Among them, compound **1** represents the first example of a C_{20}-DA glucoside. Besides, the anti-tumor activities of all the isolated compounds against human non-small-cell lung cancer A549 and H460 cells were systematically evaluated by MTT methods. The results revealed that all of the C_{19}-DAs possessed moderate activities against both of the two cell lines with IC_{50} values ranging from 7.97 to 28.42 μM, and their structure–activity relationships indicated the active sites of C-8, C-10, and C-14 positions and the nitrogen atom in the C_{19}-DA skeleton. In addition, all of the isolated DAs, with chemical structures confirmed, were further applied for network pharmacology analysis, in order to give an insight into the possible mechanisms of their anti-tumor activities. As a result, 173 potential targets and three most important pathways related to non-small-cell lung carcinoma were finally unearthed.

Introduction

Malignant tumor is one of the major diseases threatening human health with high morbidity and mortality. With the continuous development of tumor pharmacology, a deeper understanding of the process of tumorigenesis and development was achieved, which in turn facilitated the development of new therapeutic drugs. Natural products and their derivatives are always considered as one of the most important sources of drug entities for cancer treatment,[1,2] such as taxol, camptothecin, and vincristine,

which have already been applied in clinics, and also provided the leading structures for different classes of conventional anti-tumor drugs. Take camptothecin as an example, which has been proved to possess the inhibitory effect of topoisomerase I; researchers have been devoted to developing more high-efficiency and low-toxic camptothecin derivatives for treating cancer, including hydroxycamptothecin, irinotecan, topotecan, *etc.*[3] In a word, the discovery, development and further pharmacological activity investigations of new natural products and their derivatives are undoubtedly important for further development of anti-tumor agents with new structures and new mechanisms of action.

Diterpenoid alkaloids (DAs) are a kind of nitrogen-containing compounds with complex structures and significant bioactivities and toxicities, which have always aroused the scientists' interests all over the world.[4] Some DAs such as 13-acetylaconitine, lappaconitine, crassicauline A, and guanfu-base A have already been applied in the clinic as analgesic and anti-arrhythmia agents. Some DAs, including hypaconine, mesaconine, and beiwutinine, demonstrated cardiac effects,[5] while other DAs including fuziline and neoline were found to possess cardiomyocyte protective activities,[6] *etc.* Recent

[a] Shanghai Research Center for Modernization of Traditional Chinese Medicine, National Engineering Laboratory for TCM Standardization Technology, Shanghai Institute of Materia Medica, Chinese Academy of Sciences, Shanghai 201203, China. E-mail: daguo@simm.ac.cn

[b] University of Chinese Academy of Sciences, Beijing 100049, China

[c] School of Chinese Materia Medica, Nanjing University of Chinese Medicine, Nanjing 210023, China

[d] School of Traditional Chinese Pharmacy, China Pharmaceutical University, Nanjing 210009, China

† Electronic supplementary information (ESI) available. See DOI: 10.1039/d1ra04223h

research also showed that DAs could induce apoptosis of tumor cells, thus possessing potential in the development of anti-tumor agents.[7–10] DAs are mainly derived from plants of the genera *Aconitum* and *Delphinium*, and usually classified into four subtypes according to their carbon skeletons, namely C_{18}-, C_{19}-, C_{20}-, and bis-DAs.[4] More than one hundred DAs (mainly C_{19} and C_{20} subtypes) have ever been isolated from *Aconitum carmichaelii* Debx., which is a well-known traditional Chinese medicine (TCM) dubbed "fuzi" in China, and possesses significant bioactivities, including cardioactive effects, anti-arrhythmic, anti-inflammatory, and analgesic activities, *etc.*[11] It is required to be processed before oral administration to prevent poisoning, as recorded in Chinese Pharmacopoeia (2020), since the diester C_{19}-DAs would transform into monoester C_{19}-DAs and aminoalcohol C_{19}-DAs which were less toxic.[12] The structural differences between these three subtypes lie in whether an acetyl or benzoyl group substituted at the C-8 or C-14 positions, respectively, which suggested the variety of substituents also play an important part in their bioactivities and toxicities. Despite the extensive studies about DAs, there are still multitudes of DAs varied in skeletons and substituents needing to be further investigated for their activities and mechanisms of action.

This study aims at exploring more DAs with anti-tumor activities from the lateral roots of *Aconitum carmichaelii* Debx., and systematically evaluate their anti-tumor effects and possible mechanisms for future drug development. As a result, a total of thirty-seven DAs were isolated by integration of different chromatographic methods, including eight amino-alcohol-C_{19} DAs, sixteen monoester-C_{19} DAs, three diester-C_{19} DAs, one 8, 15-seco C_{19} DA, one pyro-type C_{19} DA, and eight C_{20} DAs. Among them, the structures of four new compounds, hetisane-15β-*O*-β-D-glucoside (**1**), 6-demethoxyhypaconine (**14**), carmichaeline K (**17**), and 8-*O*-ethyl-benzoyldeoxyaconine (**25**),

were determined by a combination of HR-ESI-MS, 1D NMR and 2D NMR spectra, and the NMR data of other two DAs, 8-*O*-ethyl-benzoylhypaconine (**26**)[13] and 3-deoxypyromesaconine (**37**),[14] which were reported to be synthesized previously, were also elucidated and listed in Tables S1 and S2.† The remaining 31 known compounds were all identified based on the ^{1}H NMR and ^{13}C NMR data reported in literatures, including nominine (**2**),[15] hetisine (**3**),[16] 13β-acetoxy-15β,19α-dihydroxyhetisane (**4**),[17] songorine (**5**),[18] napelline (**6**),[19] dihydroatisine (**7**),[20] trifoliolasine E (**8**),[21] karacoline (**9**),[22] isotalatizidine (**10**),[23] neoline (**11**),[24] 8-dehydroxyl-bikhaconine (**12**),[25] fuziline (**13**),[26] hypaconine (**15**),[27] mesaconine (**16**),[27] 14-benzoyltalatisamine (**18**),[28] 14-benzoylchasmanine (**19**),[29] benzoylhypaconine (**20**),[30] benzoyldeoxyaconine (**21**),[31] benzoylmesaconine (**22**),[30] benzoylaconine (**23**),[30] 14-benzoylbeiwutinine (**24**),[32] 8-*O*-ethyl-14-benzoylmesaconine (**27**),[24] 8-*O*-ethyl-14-benzoylaconine (**28**),[33] beiwucine (**29**),[34] condelphine (**30**),[35] 14-*O*-acetyltalatisamine (**31**),[36] 14-*O*-acetylneoline (**32**),[37] hypaconitine (**33**),[38] deoxyaconitine (**34**),[39] mesaconitine (**35**),[39] and nagarine A (**36**).[40] The structures of all the isolated C_{20}- and C_{19}-DAs were presented in Fig. 1 and 2, respectively. And *in vitro* systematic evaluation of their anti-tumor activities against human non-small-cell lung cancer A549 and H460 cells and non-cancerous HBE cells were conducted, their structure–activity relationships were also discussed, rendering a reference for the development of new anti-tumor agents. To further interpret the underlying mechanisms of DAs in anti-tumor activities, network pharmacology analysis was subsequently conducted for predicting the possible targets and pathways, laying the theoretical foundations for future mechanism research of DAs.

Results and discussion

Structure elucidation of new compounds

Compound **1** was purified as a white, amorphous powder, and showed a protonated molecular ion at *m/z* 460.2702 ([M + H]+,
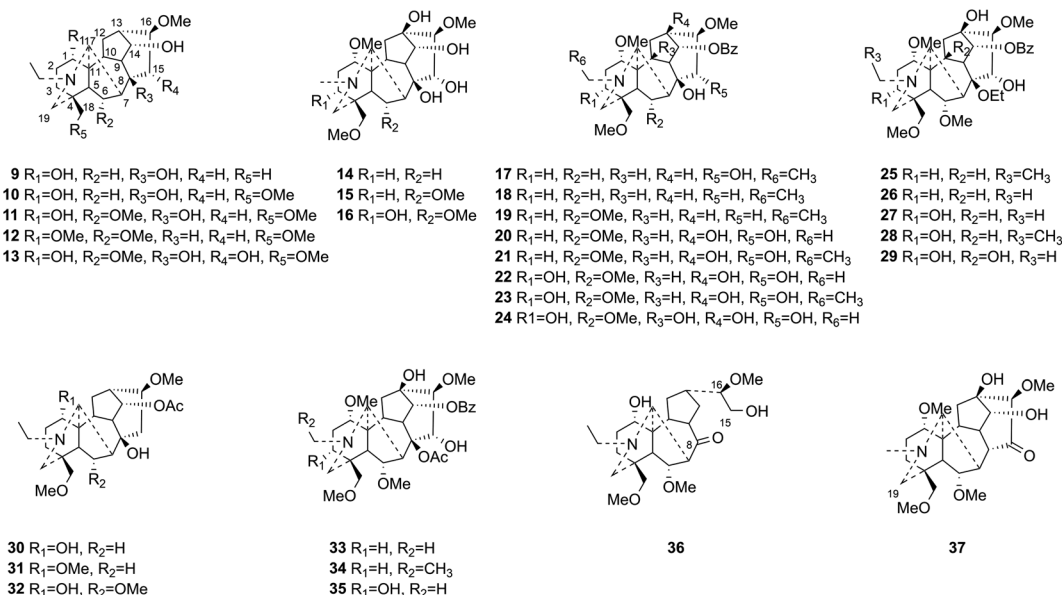

Fig. 1 The structures of C_{20}-DAs (compounds **1–8**).

9 R$_1$=OH, R$_2$=H, R$_3$=OH, R$_4$=H, R$_5$=H
10 R$_1$=OH, R$_2$=H, R$_3$=OH, R$_4$=H, R$_5$=OMe
11 R$_1$=OH, R$_2$=OMe, R$_3$=OH, R$_4$=H, R$_5$=OMe
12 R$_1$=OMe, R$_2$=OMe, R$_3$=H, R$_4$=H, R$_5$=OMe
13 R$_1$=OH, R$_2$=OMe, R$_3$=OH, R$_4$=OH, R$_5$=OMe

14 R$_1$=H, R$_2$=H
15 R$_1$=H, R$_2$=OMe
16 R$_1$=OH, R$_2$=OMe

17 R$_1$=H, R$_2$=H, R$_3$=H, R$_4$=H, R$_5$=OH, R$_6$=CH$_3$
18 R$_1$=H, R$_2$=H, R$_3$=H, R$_4$=H, R$_5$=H, R$_6$=CH$_3$
19 R$_1$=H, R$_2$=OMe, R$_3$=H, R$_4$=H, R$_5$=H, R$_6$=CH$_3$
20 R$_1$=H, R$_2$=OMe, R$_3$=H, R$_4$=OH, R$_5$=OH, R$_6$=H
21 R$_1$=H, R$_2$=OMe, R$_3$=H, R$_4$=OH, R$_5$=OH, R$_6$=CH$_3$
22 R$_1$=OH, R$_2$=OMe, R$_3$=H, R$_4$=OH, R$_5$=OH, R$_6$=H
23 R$_1$=OH, R$_2$=OMe, R$_3$=H, R$_4$=OH, R$_5$=OH, R$_6$=CH$_3$
24 R1=OH, R$_2$=OMe, R$_3$=OH, R$_4$=OH, R$_5$=OH, R$_6$=CH$_3$

25 R$_1$=H, R$_2$=H, R$_3$=CH$_3$
26 R$_1$=H, R$_2$=H, R$_3$=H
27 R$_1$=OH, R$_2$=H, R$_3$=H
28 R$_1$=OH, R$_2$=H, R$_3$=CH$_3$
29 R$_1$=OH, R$_2$=OH, R$_3$=H

30 R$_1$=OH, R$_2$=H
31 R$_1$=OMe, R$_2$=H
32 R$_1$=OH, R$_2$=OMe

33 R$_1$=H, R$_2$=H
34 R$_1$=H, R$_2$=CH$_3$
35 R$_1$=OH, R$_2$=H

36

37

Fig. 2 The structures of C$_{19}$-DAs (compounds **9–37**).

calcd for C$_{26}$H$_{38}$NO$_6$, 460.2699) in the HR-ESI-MS analysis, corresponding to the molecular formula C$_{26}$H$_{37}$NO$_6$. The NMR data (Table 1) of compound **1** demonstrated 26 carbon signals. Among them, 20 carbons including one methyl carbon (δ_C 28.59), seven methylenes, seven methines, three non-oxygenated quaternary carbons (δ_C 48.6, 44.8, 37.4), and an exocyclic double bond unit (δ_C 149.3, 111.2), constituted a typical C$_{20}$-DA skeleton.[41] And correlation of H-19 [δ_H 2.22–2.35 (2H, m)] and C-6 (δ_C 64.6) in HMBC spectrum (Fig. 3) further supported the hetisine-type C$_{20}$-DA skeleton with (C-19)–N–(C-6) connection. The other 6 carbons represented a hexose moiety consisting of five oxygenated methines [δ_H 4.36 (1H, d, J = 7.8 Hz), 2.97 (1H, t, J = 8.3 Hz), 3.09–3.14 (1H, m), 3.00–3.03 (1H, m), 3.00–3.03 (1H, m); δ_C 97.7, 73.5, 77.1, 76.8, 74.4] and an oxygenated methylene [δ_H 3.67 (1H, d, J = 11.6 Hz), 3.43–3.46 (1H, m); δ_C 61.3]. All evidences mentioned above indicated it was a hetisine-type C$_{20}$-DA with one hexose substituent. The only one oxygenated carbon signal (δ_C 74.3) in the skeleton was assigned to C-15 based on the HMBC correlation from H-15 [δ_H 4.13 (1H, s)] to C-1′ (δ_C 97.75) and C-17 (δ_C 111.2). Besides, correlation of H-17 [δ_H 4.86 (1H, s)] with H-15, and H-1′ [δ_H 4.36 (1H, d, J = 7.8 Hz)] in NOESY spectrum implied the β-configuration of 15-glucoside. And the vicinal coupling constant value of H-1′ and H-2′ [δ_H 2.97 (1H, t, J = 8.3 Hz)], and NOESY correlation between H-4′ [δ_H 3.00–3.03 (1H, m)] and H-6′ [δ_H 3.67 (1H, d, J = 11.6 Hz)] indicated the hexose was a β-glucoside. In addition, the D,L-configuration of the glucoside was determined by acid hydrolysis and then derivatization, as reported in literature.[42] By comparing its UHPLC-MS chromatogram (Fig. S9†) with glucoside derivatives prepared in the same way, structure of compound **1** was fully established and named as hetisane-15β-O-β-D-glucoside. Since the previously reported glycosidic DAs all bear a C$_{19}$-skeleton,[43,44] this is the first C$_{20}$-DA glycoside isolated from *Aconitum carmichaelii* Debx.

Compound **14a** (the acetate salt of compound **14**) was obtained as a white, amorphous powder, and its molecular formula was determined to be C$_{23}$H$_{37}$NO$_7$ by HR-ESI-MS data at m/z 440.2636 ([M-CH$_3$COO$^-$]$^+$, calcd for C$_{23}$H$_{38}$NO$_7$, 440.2648),

Table 1 ^{1}H (500 MHz) and ^{13}C (125 MHz) NMR data of compound **1** in DMSO-d$_6$

| Position	δ_H (ppm)	δ_C (ppm)
1	1.91–1.98 (1H, m); 1.12–1.26 (1H, m)	26.8
2	1.48–1.55 (2H, m)	19.3
3	1.36–1.40 (1H, m); 1.12–1.26 (1H, m)	33.9
4	—	37.4
5	2.44 (1H, s)	74.4
6	3.07 (1H, s)	64.6
7	1.97 (1H, dd, J = 13.3, 2.6 Hz); 1.41–1.46 (1H, m)	32.6
8	—	48.6
9	1.66–1.74 (1H, m)	42.1
10	—	44.8
11	1.58–1.66 (1H, m); 1.05–1.10 (1H, m)	35.0
12	2.07–2.13 (1H, m)	33.2
13	1.66–1.74 (1H, m); 1.55–1.58 (1H, m)	24.3
14	1.75–1.83 (1H, m)	44.1
15	4.13 (1H, s)	74.3
16	—	149.3
17	4.99 (1H, s); 4.86 (1H, s)	111.2
18	0.91 (3H, s)	28.6
19	2.22–2.35 (2H, m)	62.1
20	1.36 (1H, s)	60.9
1′	4.36 (1H, d, J = 7.8 Hz)	97.7
2′	2.97 (1H, t, J = 8.3 Hz)	73.5
3′	3.09–3.14 (1H, m)	77.1
4′	3.00–3.03 (1H, m)	76.8
5′	3.00–3.03 (1H, m)	74.4
6′	3.67 (1H, d, J = 11.6 Hz); 3.43–3.46 (1H, m)	61.3
2′-OH	4.64–4.69 (1H, m)	—
3′-OH	4.88–4.91 (1H, m)	—
4′-OH	4.88–4.91 (1H, m)	—
6′-OH	4.44–4.50 (1H, m)	—
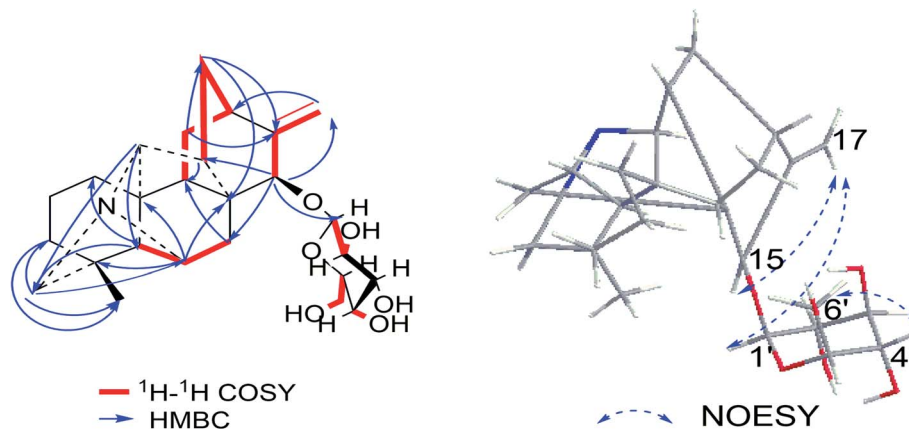
Fig. 3 Key HMBC, ^1H–^1H COSY and NOESY correlations of compound **1**.

indicative of six degrees of unsaturation. The ^{13}C NMR spectra displayed 25 carbon signals, including the characteristic signals attributed to one *N*-methyl group [δ_H 2.29 (3H, s), δ_C 42.9], three methoxy groups [δ_H 3.27(3H, s), δ_C 56.8; δ_H 3.62 (3H, s), δ_C 61.1; δ_H 3.28(3H, s), δ_C 59.6], and one acetyl group [δ_C 172.8; δ_H 2.01 (3H, s), δ_C 22.8]. Except for the above signals, the remaining 19 carbon signals, constituting six methylenes, nine methines, and four quaternary carbons, revealed that compound **14a** was a C_{19}-DA.[45] Considering that DAs usually display protonated ions in HR-ESI-MS spectrum, the number of carbons calculated from

HR-ESI-MS data are supposed to be consistent with those displayed in ^{13}C NMR spectrum, compound **14a** might be a salt due to the acidic conditions used in the isolation process. And because the acetyl unit had no correlations with other signals in either HMBC or ROESY spectrum (Fig. 4), it might be an acetate. Besides, the HMBC correlations between 18-OMe [δ_H 3.28 (3H, s)] and the methylene carbon C-18 (δ_C 79.7), 1-OMe [δ_H 3.27 (3H, s)] and C-1 (δ_C 85.8), 16-OMe [δ_H 3.62 (3H, s)] and C-16 (δ_C 91.3) indicated the three methoxy groups were substituted at C-18, C-1, and C-16, respectively. It was also speculated to contain four
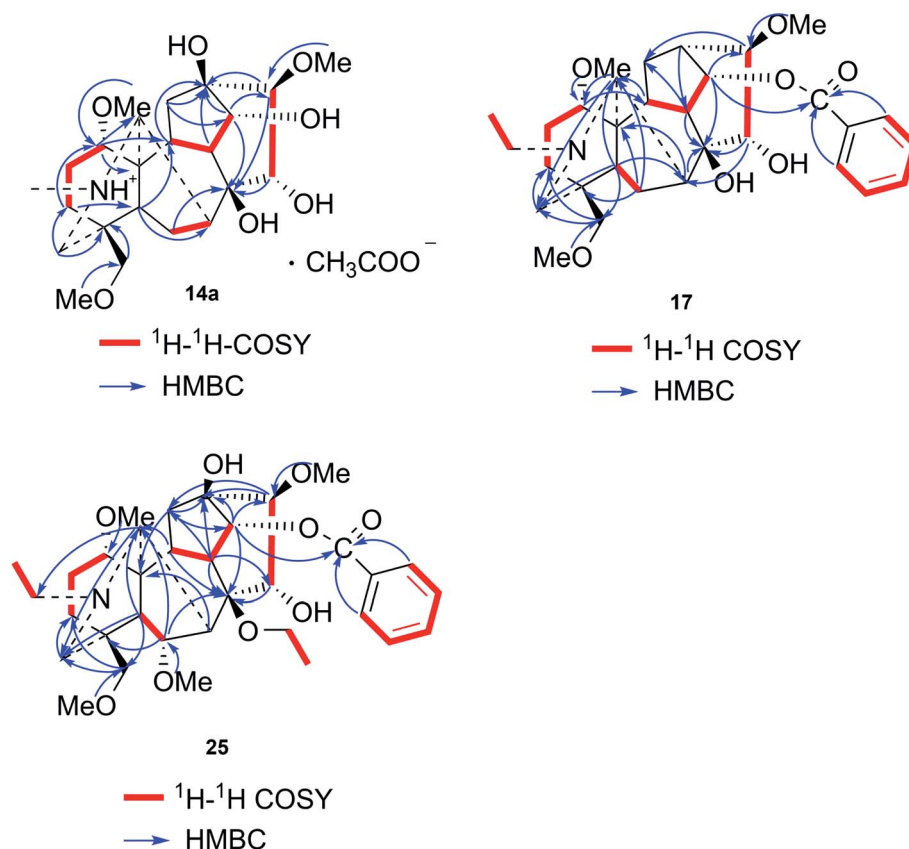

Fig. 4 Key ^1H–^1H COSY and HMBC correlations of compounds **14a**, **17** and **25**.
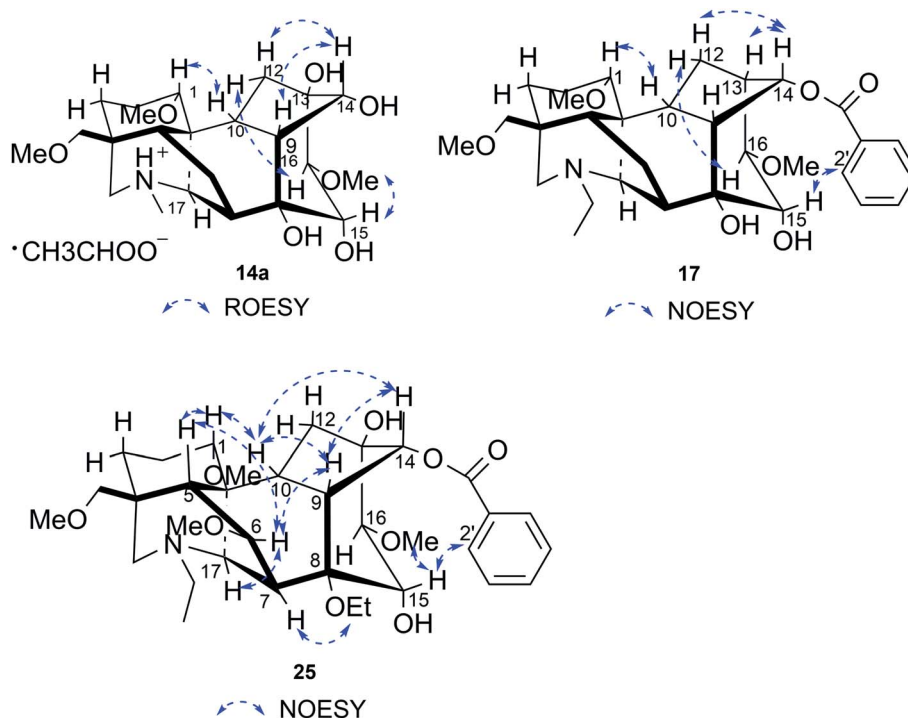
Fig. 5 Key NOESY/ROESY correlations of compounds **14a**, **17** and **25**.

hydroxy groups according to the seven oxygenated carbon signals observed in the ^{13}C NMR spectrum. And the doublet peak of H-14 [δ_H 3.93 (1H, d, $J = 5.1$ Hz)], the ^1H–^1H COSY cross-peaks of H-14/H-10 [δ_H 1.87–1.95 (1H, m)]/H-9 [δ_H 2.29–2.34 (1H, m)], H-15 [δ_H 4.38–4.49 (1H, m)]/H-16 [δ_H 3.16 (1H, d, $J = 5.8$ Hz)], and the HMBC correlations of H-6a [δ_H 1.79–1.87 (1H, m)], H-14, H-15, H-16 with C-8 (δ_C 79.0), and H-9, H-10, H-12b [δ_H 1.96–1.98 (1H, m)], H-14, H-16 with C-13 (δ_C 74.71) implied the four hydroxy groups were located at the oxygenated quaternary carbon C-8, C-13, and the oxygenated methine carbon C-14 (δ_C 79.0) and C-15 (δ_C 82.4), respectively. After the planar structure of compound **14a** was constructed, its relative configuration was also deduced from the ROESY spectrum (Fig. 5). ROE correlations of H-1 [δ_H 3.06 (1H, dd, $J = 10.5, 6.7$ Hz)] with H-10β, and H-14 with H-9β indicated the α-configurations of 1-OMe and 14-OH, respectively, while correlations of one proton of H-12 [δ_H 1.96–1.98 (1H, m)] with H-14, and another proton of H-12 [δ_H 2.72 (1H, dd, $J = 13.6, 4.1$ Hz)] with H-16, and H-15 with 16-OMe implied the β-configuration of 16-OMe and α-configuration of 15-OH. At last, compound **14** (5 mg) was obtained as a free base by further alkaline treatment of compound **14a** using preparative TLC (*n*-hexane–ethyl acetate–diethylamine, 5 : 2 : 1). By comparing their ^1H NMR and ^{13}C NMR data (Table 2), compound **14a** was confirmed to be an acetate, and named as 6-demethoxyhypaconine acetate, while compound **14** was named as 6-demethoxyhypaconine, and its structure was presented in Fig. 1.

Compound **17** was isolated as a white, amorphous powder with a molecular formula of $C_{31}H_{43}NO_7$, as deduced from the HR-ESI-MS data at m/z 542.3129 ([M + H]$^+$, calcd for $C_{31}H_{44}NO_7$, 542.3118). The NMR data (Table 2) verified compound **17** was

substituted with one *N*-ethyl group [δ_H 2.68–2.78 (1H, m), 2.40–2.47 (1H, m), 1.09 (3H, t, $J = 7.2$ Hz); δ_C 49.7, 13.4], three methoxy groups [δ_H 3.29 (3H, s), δ_C 59.6; δ_H 3.37 (3H, s), δ_C 57.1; 3.31 (3H, s), δ_C 56.4], one benzoyl group [δ_H 7.49–7.55 (1H, m), 7.98–8.03 (2H, m), 7.37–7.44 (2H, m); δ_C 166.4, 133.0, 130.3, 129.8 × 2, 128.6 × 2]. The remaining 19 carbons, comprising six methylenes, ten methines, and three quaternary carbons, suggested it was a typical C_{19}-DA.[41] Besides, the 6 oxygenated carbons, indicated the substitution of another two hydroxy groups, except for the three methoxy groups and one benzoyl group. HMBC cross-peaks of the three methoxy groups (δ_H 3.31, 3.37, 3.29) with correlated carbons attested their substitutions at C-1 (δ_C 85.3), C-16 (δ_C 90.7), and the methylene carbon C-18 (δ_C 79.6), respectively. And correlations between signals of H-14 [δ_H 5.07 (1H, t, $J = 4.8$ Hz)] and the ester carbonyl carbon (δ_C 166.4) obtained from HMBC spectrum revealed the substitution of benzoyl group at C-14 (δ_C 76.9). Moreover, ^1H–^1H COSY cross-peak between H-15 [δ_H 4.39 (1H, d, $J = 6.7$ Hz)] and H-16 [δ_H 3.09 (1H, d, $J = 6.7$ Hz)] indicated a hydroxyl group located at C-15 (δ_C 79.9). And another hydroxyl group was speculated to be placed at C-8 (δ_C 78.3) based on the long-range correlations of the oxygenated quaternary carbon C-8 with H-7 [δ_H 2.58 (1H, s)], H-9 [δ_H 2.47–2.49 (1H, m)], H-14, and H-15 in HMBC spectrum. In addition, the relative configuration of compound **17** was established by NOE correlations between H-1 [δ_H 3.20 (1H, m)] and H-10β [δ_H 1.98–2.07 (1H, m)], H-14 and H-13β [δ_H 2.52–2.56 (1H, m)], and between H-15 and H-2′, 6′ [δ_H 7.98–8.03 (2H, m)], indicating the α-configurations of 1-OMe, 14-OH, and 15-OH, respectively. And correlations of one proton at C-12 [δ_H 1.98–2.07 (1H, m)] with H-14, and another proton at C-12 [δ_H 2.47–2.49 (1H, m)] with H-16 implied the β-configuration of 16-OMe.

Paper

Table 2 ^{1}H and ^{13}C NMR data of compounds **14**, **14a**, **17**, and **25** in CDCl$_3$

Position	14[a] δ_H (ppm)	δ_C (ppm)	14a[b] δ_H (ppm)	δ_C (ppm)	17[a] δ_H (ppm)	δ_C (ppm)	25[b] δ_H (ppm)	δ_C (ppm)
1	3.05–3.10 (1H, m)	85.7	3.06 (1H, dd, J = 10.5, 6.7 Hz)	85.8	3.17–3.23 (1H, m)	85.3	3.28–3.31 (1H, m)	83.4
2	2.16–2.20 (1H, m); 2.04–2.09 (1H, m)	26.6	2.12–2.26 (1H, m); 2.03–2.06 (1H, m)	26.7	2.23–2.34 (1H, m); 1.91–1.98 (1H, m)	26.1	2.09–2.19 (1H, m); 1.53–1.65 (1H, m)	24.2
3	1.72–1.80 (1H, m); 1.38–1.49 (1H, m)	32.7	1.71–1.79 (1H, m); 1.35–1.48 (1H, m)	32.7	1.71–1.78 (1H, m); 1.48–1.56 (1H, m)	32.0	1.82–1.95 (1H, m); 1.65–1.76 (1H, m)	31.2
4	—	38.5	—	38.7	—	38.4	—	38.7
5	1.50–1.64 (1H, m)	45.0	1.58 (1H, d, J = 8.1 Hz)	45.0	1.68 (1H, d, J = 7.5 Hz)	45.0	2.23–2.25 (1H, m)	44.8
6	1.82–1.89 (1H, m); 1.54–1.64 (1H, m)	24.8	1.79–1.87 (1H, m); 1.52–1.56 (1H, m)	24.8	1.87 (1H, dd, J = 15.0, 7.6 Hz); 1.62 (1H, dd, J = 15.0, 8.4 Hz)	25.0	4.09 (1H, d, J = 6.4 Hz)	82.6
7	2.36–2.47 (1H, m)	38.7	2.44 (1H, d, J = 8.1 Hz)	38.7	2.58 (1H, s)	40.4	2.88 (1H, s)	43.7
8	—	79.0	—	79.0	—	78.3	—	82.6
9	2.31–2.34 (1H, m)	47.9	2.29–2.34 (1H, m)	47.8	2.47–2.49 (1H, m)	45.5	2.60–2.68 (1H, m)	44.8
10	1.91–1.96 (1H, m)	42.1	1.87–1.95 (1H, m)	42.3	1.98–2.07 (1H, m)	45.4	2.09–2.19 (1H, m)	40.9
11	—	48.7	—	48.7	—	49.1	—	50.6
12	2.66–2.73 (1H, m); 1.97–2.01 (1H, m)	37.1	2.72 (1H, dd, J = 13.6, 4.1 Hz); 1.96–1.98 (1H, m)	37.2	2.47–2.49 (1H, m); 1.98–2.07 (1H, m)	29.7	2.20–2.23 (2H, m)	36.7
13	—	76.7	—	76.8	2.52–2.56 (1H, m)	37.9	—	74.8
14	3.96 (1H, d, J = 5.1 Hz)	79.3	3.93 (1H, d, J = 5.1 Hz)	79.0	5.07 (1H, t, J = 4.8 Hz)	76.9	4.83 (1H, d, J = 5.1 Hz)	79.3
15	4.39–4.50 (1H, m)	83.1	4.38–4.49 (1H, m)	82.4	4.39 (1H, d, J = 6.7 Hz)	79.9	4.59 (1H, d, J = 5.5 Hz)	77.7
16	3.17 (1H, d, J = 5.6 Hz)	90.8	3.16 (1H, d, J = 5.8 Hz)	91.3	3.09 (1H, d, J = 6.7 Hz)	90.7	3.34–3.38 (1H, m)	93.1
17	3.02 (1H, s)	62.9	2.99 (1H, s)	62.8	3.07 (1H, s)	62.3	3.29 (1H, s)	63.3
18	3.11 (1H, d, J = 9.0 Hz); 2.97 (1H, d, J = 9.0 Hz)	79.6	3.11 (1H, d, J = 9.0 Hz); 2.96 (1H, d, J = 9.0 Hz)	79.7	3.12 (1H, d, J = 9.2 Hz); 3.01 (1H, d, J = 9.2 Hz)	79.6	3.58 (1H, d, J = 8.2 Hz); 3.18 (1H, d, J = 8.2 Hz)	79.2
19	2.34–2.36 (1H, m); 2.01–2.04 (1H, m)	55.9	2.38 (1H, d, J = 11.6 Hz); 1.99–2.02 (1H, m)	55.8	2.56–2.57 (1H, m); 2.07–2.14 (1H, m)	53.6	3.02–3.10 (1H, m); 2.85–2.91 (1H, m)	55.3
NCH$_3$	2.31 (3H, s)	42.9	2.29 (3H, s)	42.9	—	—	—	—
N$\underline{CH_2}$CH$_3$	—	—	—	—	2.68–2.78 (1H, m); 2.40–2.47 (1H, m)	49.7	3.34–3.38 (1H, m); 2.92–3.01 (1H, m)	50.1
NCH$_2$$\underline{CH_3}$	—	—	—	—	1.09 (3H, t, J = 7.2 Hz)	13.4	1.29 (3H, t, J = 5.5 Hz)	12.3
1-OMe	3.28 (3H, s)	56.9	3.27 (3H, s)	56.8	3.31 (3H, s)	56.4	3.34 (3H, s)	56.3
6-OMe	—	—	—	—	—	—	3.27 (3H, s)	58.8
8-O$\underline{CH_2}$CH$_3$	—	—	—	—	—	—	3.46–3.50 (1H, m); 3.38–3.44 (1H, m)	57.5
8-OCH$_2$$\underline{CH_3}$	—	—	—	—	—	—	0.56 (3H, t, J = 6.9 Hz)	15.3
16-OMe	3.62 (3H, s)	60.8	3.62 (3H, s)	61.1	3.37 (3H, s)	57.1	3.79 (3H, s)	62.0
18-OMe	3.29 (3H, s)	59.6	3.28 (3H, s)	59.6	3.29 (3H, s)	59.6	3.31 (3H, s)	59.3
14-OCOC$_6$H$_5$	—	—	—	—	—	166.4	—	166.4
1'	—	—	—	—	—	130.3	—	130.3
2'	—	—	—	—	7.98–8.03 (1H, m)	129.8	8.02–8.07 (1H, m)	129.9
3'	—	—	—	—	7.37–7.44 (1H, m)	128.6	7.45 (1H, t, J = 7.7 Hz)	128.5
4'	—	—	—	—	7.49–7.55 (1H, m)	133.0	7.53–7.59 (1H, m)	133.1
5'	—	—	—	—	7.37–7.44 (1H, m)	128.6	7.45 (1H, t, J = 7.7 Hz)	128.5
6'	—	—	—	—	7.98–8.03 (1H, m)	129.8	8.02–8.07 (1H, m)	129.9
$\underline{CH_3}$COO$^-$	—	—	—	172.8	—	—	—	—
$\underline{CH_3}$COO$^-$	—	—	2.01 (3H, s)	22.8	—	—	—	—

^{a} In ^{1}H (600 MHz) and ^{13}C (150 MHz) NMR. ^{b} In ^{1}H (500 MHz) and ^{13}C (125 MHz) NMR.

Accordingly, the structure of compound **17** was determined as shown in Fig. 2, and was named as carmichaeline K, which was isolated as a free base for the first time in this study, compared with the previously reported carmichaeline K trifluoroacetate.[32,46–48] And the main differences of their NMR spectra lie in the chemical shifts of N − CH$_2$CH$_3$ group, which were δ_H 1.09 (3H, t, J = 7.2 Hz) and δ_C 13.4 for compound **17**, while δ_H 1.36–1.58 and δ_C 10.0–11.4 for the corresponding salts.

Compound **25** was isolated as a white, amorphous powder, and its molecular formula was established as C$_{34}$H$_{49}$NO$_9$ based on its HR-ESI-MS data at m/z 616.3509 ([M + H]$^+$, calcd for C$_{34}$H$_{50}$NO$_9$, 616.3486). The NMR signals (Table 2) implied the existence of one N-ethyl group [δ_H 3.34–3.38 (1H, m), 2.92–3.01 (1H, m), 1.29 (3H, t, J = 5.5 Hz); δ_C 50.1, 12.3], four methoxy groups [δ_H 3.34 (3H, s), δ_C 56.3; δ_H 3.27 (3H, s), δ_C 58.8; δ_H 3.79 (3H, s), δ_C 62.0; δ_H 3.31 (3H, s), δ_C 59.3], one benzoyl group [δ_H

8.02–8.07 (2H, m), 7.45 (2H, t, $J = 7.7$ Hz), 7.53–7.59 (1H, m); δ_C 166.4, 130.3, 129.9 × 2, 128.5 × 2, 133.1] and one ethoxy group [δ_H 3.46–3.50 (1H, m), 3.38–3.44 (1H, m), 0.56 (3H, t, $J = 6.9$ Hz); δ_C 57.5, 15.3]. The remaining 19 carbons, including 8 oxygenated carbons, constituted the skeleton of C_{19}-DA,[45] and indicated the substitution of two hydroxy groups. The locations of four methoxy groups and one benzoyl group were confirmed according to the correlation signals of H-1/H-2/H-3, H-5/H-6, and H-14/H-9/H-10 in ^{1}H–^{1}H COSY spectrum, as well as the HMBC correlations between signals of 1-OMe [δ_H 3.34 (3H, s)], 6-OMe [δ_H 3.27 (3H, s)], 16-OMe [δ_H 3.79 (3H, s)], 18-OMe (δ_H 3.31), H-14 [δ_H 4.83 (1H, d, $J = 5.1$ Hz)] and C-1 (δ_C 83.4), C-6 (δ_C 82.6), C-16 (δ_C 93.1), C-18 (δ_C 79.2), 14-OBz (δ_C 166.4), respectively. One hydroxy group was attached to C-15 (δ_C 77.7) based on the H-15/H-16 correlation in ^{1}H–^{1}H COSY spectrum, and the other one attached to C-13 (δ_C 74.8) according to the doublet peak of H-14, and HMBC correlations of H-9 [δ_H 2.60–2.68 (1H, m)], H-12 [δ_H 2.20–2.23 (2H, m)], H-14, and H-16 [3.34–3.38 (1H, m)] with C-13 (δ_C 74.8). Besides, the ethoxy group was placed at the oxygenated quaternary carbon C-8 (δ_C 82.6) according to the HMBC correlations from H-6 [δ_H 4.09 (1H, d, $J = 6.4$ Hz)], H-9, H-10 [2.15 (1H, m)], H-14, and H-15 [δ_H 4.59 (1H, d, $J = 5.5$ Hz)] to C-8 (δ_C 82.6), and the NOE correlation of H-7 [δ_H 2.88 (1H, s)] to 8-OCH$_2$CH$_3$ [δ_H 3.48 (1H, m)]. In addition, NOESY cross-peaks of H-1/H-5β, and H-10β; H-6/H-5β, H-9β, and H-17β; H-14/H-9β, and H-10β; H-15/H-2′, 6′, and 16-OMe indicated that 1-OMe, 6-OMe, 14-OBz, and 15-OH took α-configurations, while 16-OMe was β-configuration. Consequently, as exhibited in Fig. 2, compound **25** was assigned as 8-O-ethyl-benzoyldeoxyaconine.

In order to verify whether these compounds were artifacts, the powdered dried lateral roots of *Aconitum carmichaelii* Debx. were also extracted by 1% hydrochloric acid (HCl) containing water, and the HR-ESI-MS spectrum showed compounds **25–29** with an oxyethyl group substituted at C-8 position were artificial products, which could be produced in the presence of ethanol according to previous reports.[32]

Anti-tumor activity assay

Anti-tumor activities of all the isolated compounds and the positive drug 5-fluorouracil (5-FU) against human non-small-cell lung cancer A549 and H460 cells and non-cancerous HBE cells were examined, the IC$_{50}$ values expressed as means ± s.d. from three independent experiments were listed in Table 3, and representative IC$_{50}$ curves for each compound were displayed in Fig. S53.† It could be concluded that all the C_{19} DAs showed moderate inhibitory activities against both of the two cancerous cell lines with IC$_{50}$ values in the range of 7.97–28.42 μM, while all the C_{20}-DAs only exhibited moderate activities against H460 cells with IC$_{50}$ values from 13.56 to 27.44 μM, but several C_{20}-DAs seemed to possess little inhibition against A549 cells, displaying IC$_{50}$ values of more than 30 μM. Besides, most of the DAs displayed selectivity towards one or both of the two cancerous cell lines over non-cancerous cell line to some extent, and several compounds such as compounds **9, 25**, *etc.* exhibited higher selectivity. Furthermore, the predicted properties for compound **9** also fall within the Lipinski's rule of five, with molecular weight 377.52, 3 hydrogen bond donors, 5 hydrogen bond acceptors, 5 freely rotatable bonds and log *P* value 1.278 ± 0.521. And its ADME parameters predicted by a web-based application PreADMET (https://preadmet.bmdrc.kr/) also indicated its moderate absorption and bioavailability, including the permeability of Caco-2 cell (value of 15.54), percentage of human intestinal absorption (HIA, value of 88.24), and skin permeability (value of −5.58) to estimate absorption, blood brain barrier (BBB, value of 0.31) and plasma protein binding (PPB, value of 29.33) for drug penetration, *etc.* On basis of these results, DAs and their derivatives, especially those with the C_{19}-skeletons, may have the potentials for future development of anti-tumor agents. Besides, their physicochemical properties, biochemical properties, pharmacokinetic and pharmacodynamic parameters including ADMET and so on also need to be further evaluated.

Table 3 IC$_{50}$ values (μM) of compounds **1–37** against HBE, A549 and H460 cell lines

Compound	HBE	A549	H460	Compound	HBE	A549	H460
1	37.86 ± 2.16	48.10 ± 11.65	27.44 ± 0.55	**20**	30.66 ± 10.14	21.54 ± 2.86	21.79 ± 2.11
2	39.91 ± 6.20	75.30 ± 12.48	24.33 ± 1.66	**21**	25.66 ± 3.72	16.07 ± 0.73	24.06 ± 4.74
3	21.77 ± 2.24	17.65 ± 1.35	14.14 ± 0.80	**22**	32.80 ± 3.66	25.95 ± 10.25	22.31 ± 1.04
4	36.47 ± 2.49	16.49 ± 0.29	24.14 ± 1.71	**23**	28.74 ± 1.05	20.60 ± 0.25	18.90 ± 4.45
5	32.41 ± 2.62	21.24 ± 0.84	25.10 ± 0.59	**24**	21.56 ± 0.99	17.09 ± 2.08	13.48 ± 1.00
6	28.76 ± 2.36	25.24 ± 0.25	20.94 ± 0.68	**25**	50.07 ± 9.82	12.58 ± 1.82	12.76 ± 2.10
7	21.59 ± 8.19	13.67 ± 0.47	13.56 ± 0.23	**26**	25.51 ± 2.22	14.49 ± 0.71	13.87 ± 0.67
8	43.72 ± 4.39	64.16 ± 1.70	26.46 ± 3.08	**27**	30.21 ± 1.28	17.61 ± 1.17	18.81 ± 1.57
9	49.74 ± 8.11	8.28 ± 0.41	9.69 ± 0.40	**28**	31.35 ± 2.62	20.13 ± 0.73	18.31 ± 1.07
10	21.38 ± 1.18	8.33 ± 0.20	12.23 ± 0.97	**29**	32.09 ± 1.85	17.82 ± 1.00	19.38 ± 4.82
11	24.30 ± 2.18	17.09 ± 3.69	12.72 ± 3.68	**30**	31.43 ± 6.00	16.36 ± 2.38	16.00 ± 1.15
12	21.15 ± 0.72	8.36 ± 0.82	9.92 ± 0.71	**31**	27.73 ± 0.98	18.46 ± 2.03	22.22 ± 2.58
13	26.21 ± 3.78	12.25 ± 1.05	10.70 ± 1.60	**32**	29.63 ± 1.73	24.56 ± 3.24	18.50 ± 1.58
14	27.31 ± 3.65	18.16 ± 1.32	22.80 ± 0.81	**33**	32.70 ± 4.56	14.31 ± 1.79	16.52 ± 2.22
15	24.84 ± 2.50	12.33 ± 1.59	13.69 ± 0.77	**34**	30.99 ± 4.80	14.87 ± 4.02	14.64 ± 1.32
16	20.20 ± 1.83	8.92 ± 0.86	7.97 ± 0.31	**35**	26.31 ± 0.98	13.01 ± 5.69	15.55 ± 4.84
17	31.03 ± 10.73	21.30 ± 3.27	22.30 ± 2.16	**36**	26.85 ± 0.62	26.46 ± 0.86	28.42 ± 8.89
18	44.53 ± 13.56	25.43 ± 9.64	23.36 ± 2.35	**37**	32.59 ± 5.94	19.43 ± 1.57	14.41 ± 0.64
19	34.11 ± 2.88	13.88 ± 0.52	15.69 ± 0.18	**5-FU**	8.93 ± 6.05	12.52 ± 8.81	6.16 ± 1.80

Structure–activity relationship

The structure–activity relationships of the isolated C_{19}-DAs were discussed based on the comprehensive analysis of different types and positions of their substituents, as well as the IC_{50} values against A549 and H460 cells. First of all, it is obvious that substituents at C-8 position exerted an influence on the anti-tumor activities of C_{19}-DAs. The diester C_{19}-DAs with an acetyl group attached to the C-8 position showed stronger activities than monoester C_{19}-DAs with the hydroxy group, as indicated by comparison of compounds **33**, **34** and **35** with compounds **20**, **21**, and **22**, respectively, which is similar with those reported in literatures.[8] Furthermore, when the hydroxy group at C-8 position was further replaced by an ethoxy group, such as in compounds **25–27**, the inhibitory activities were also strengthened. Besides, the hydroxy group at C-10 position displayed a slight increase in anti-tumor activities of C_{19}-DAs, as illustrated by compounds **24** and **29**, compared with compounds **22** and **27**. On top of that, the replacement of the 14-acetyl or benzoyl with the hydroxy group also leads to the improvement in inhibitory activities on A549 and H460 cells, which was attested by pairs of compounds **10** and **30**, **11** and **32**, **15** and **20**, **16** and **22**. Additionally, slight decrease was observed in the anti-tumor activities of *N*-methyl substituted compounds **20**, **22**, **26**, and **27**, than *N*-ethyl substituted compounds **21**, **23**, **25**, and **28**, suggesting that substituents at nitrogen atom of C_{19}-DAs have slight effects on their anti-tumor activities against A549 and H460 cells. However, hydroxy group substituted at C-3 position seemed to exert no significant effects on the anti-tumor activities of C_{19}-DAs, by comparing the IC_{50} values of compounds **20** with **22**, and **33** with **35**. Based on all of the above evidences, it is concluded that C-8 and C-14 positions of C_{19}-DAs are active sites which could be replaced by different substituents for development of potential anti-tumor agents. Besides, substituents at C-10 position and nitrogen atom may also slightly alter the anti-tumor activities of C_{19}-DAs.

Network pharmacology analysis

All of the isolated DAs, with chemical structures confirmed, were further applied for network pharmacology analysis to explore the possible mechanisms of their anti-tumor activities. Compound-associated-target prediction was firstly performed by screening the metaTarFisher (https://metatarget.scbdd.com/) search server which integrated more than 10 popular target fishing tools, resulting in discovery of 362 target genes. Meanwhile, DisGeNET platform was also applied for discovery of 3926 genes closely related with non-small-cell lung carcinoma. The intersection of these compound-associated genes and disease-associated genes generated 173 potential target genes, which was further used for protein–protein interaction (PPI) analysis by STRING database to search for the proteins that may jointly contribute to a function as well as the core proteins which may play a pivotal role in the entire network, according to the PPI network node degree value, as depicted in Fig. 6 and listed in Table S3.† Furthermore, GO/KEGG enrichment analysis was performed on Metascape platform to reveal the most important KEGG pathways, reactome gene sets and GO
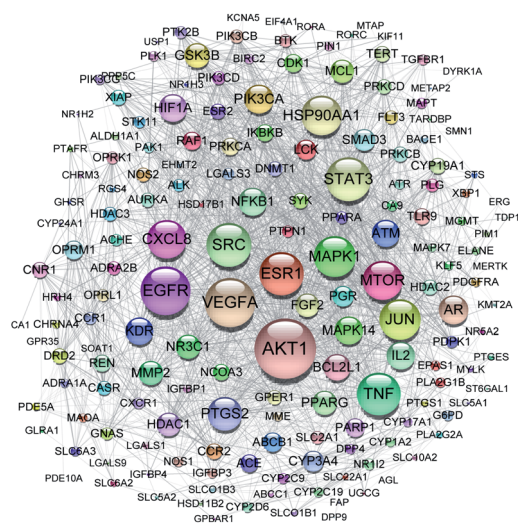

Fig. 6 PPI network of 173 target genes. The size of the target genes represented the node degree value.

biological processes involved in their bioactivities. According to the Qvalues (Table S4† and Fig. 7), "pathways in cancer", "signaling by interleukins" and "regulation of MAPK cascade" were the three most important pathways related to their anti-tumor effects. Moreover, the whole "compound-target-disease" network was constructed in Cytoscape software to demonstrate the potential anti-tumor mechanisms of DAs in treating cancer, as represented in Fig. 8.

Based on the above target genes and related pathways, the underlying anti-tumor mechanisms of DAs might be explained in the following aspects. Firstly, pathways in cancer, especially the PI3K-AKT signaling pathway, according to the target genes (AKT1, PIK3CA, PIK3CB, PIK3CD, mTOR, *etc.*) involved, as listed in Table S4,† which plays a crucial part in tumor progression.[49] PI3K was activated when stimulated by upstream signals, such as TGF, EGF, PDGF, FLT3 and so on, and further activated AKT and various downstream signaling molecules, including NF-κB, mTOR, eNOS, VEGF, GSK3β, *etc.* to regulate the proliferation,
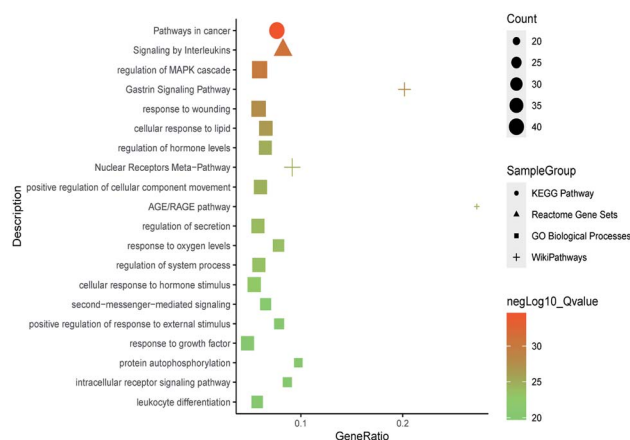

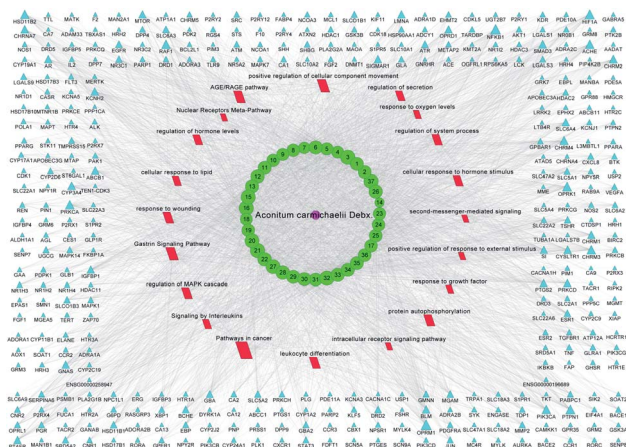**Fig. 7** Bubble graph demonstrating GO/KEGG enrichment analysis results.

Fig. 8 Visualization of "compound-target-pathway" network. The purple octagon-shaped node represented *Aconitum carmichaelii* Debx., the green ellipse-shaped node represented the DA compounds **1–37**, the blue triangle-shaped node represented the target genes, the red parallelogram-shaped node represented the pathways, while the size of the node represented the degree value.

invasion and metastasis, apoptosis, angiogenesis and carbohydrate metabolism of tumor cells.[50] By inhibiting the expression of various molecules in the pathway, the growth and metastasis of tumors can be inhibited, and various therapeutic drugs targeting this pathway have been continuously developed and used in pre-clinical research and clinical trials for tumor treatment.[51] DAs and their derivatives may also have the anti-tumor effects by blocking the PI3K-AKT signaling pathway.

Besides, DAs were also associated with signaling by interleukins. Interleukins were first identified as cytokines interacting between leukocytes during immune responses, further studies showed they could also take part in regulations of many other cells throughout the body, and play an important role in tumor immunobiology.[52] For example, IL-2 exerted an influence on cell growth and activation, and showed clinical efficacy in both solid tumors and hematologic malignancies.[53] Therefore, DAs may have potentials in treating cancer by influencing interleukins signals.

Moreover, DAs may also influence cell proliferation, differentiation, apoptosis, metastasis, and invasion by regulation of MAPK cascade, which mainly contains four main families, ERKs, p38MAPKs, JNKs, and ERK5.[54] Among them, ERK1/2 were activated abnormally in a variety of tumors after phosphorylation, and acted on certain regulatory factors to promote cell proliferation, inhibit cell apoptosis, and regulate cell cycle.[55] Many chemotherapeutic drugs inhibit the growth of tumors by inhibiting the activation of ERK. Some research also found the activation of ERK-MAPK transduction pathway could activate downstream tumor suppressor genes and initiate the p53-dependent apoptosis pathway to inhibit tumor growth.[56] Besides, the mechanism of DAs in regulation of MAP kinase activity was also supported by previous report that *Aconitum* species played an anti-tumor role by inducing apoptosis of A549 cells through the activation of p38 MAPK-pathway.[7]

In summary, DAs may inhibit tumor cell growth and promote apoptosis by regulating different signal transduction

pathways including the PI3K-AKT signaling pathway, interleukins signaling pathways, MAPK signaling pathway, *etc.* And the whole mechanism network formed by their intricate relationships ultimately determines the survival and apoptosis of tumor cells, which deserves further investigation.

Experimental section

General experimental procedures

The optical rotation data were determined on an Autopol VI Automatic Polarimeter (Rudolph Research Analytical, Hackettstown, NJ, USA). The IR spectra in the range of 4000–650 cm^{-1} were recorded on a Nicolet iS50 FTIR spectrometer using a Diamond ATR module and processed by OMNIC v9.7.7 software (Thermo Fisher Scientific, Waltham, MA, USA). HR-ESI-MS analysis were conducted on Waters UPLC HClass system and Xevo QTOF mass spectrometer (Waters Corporation, Milford, MA, USA) using a Waters CSH C18 column (100 mm × 2.1 mm, 1.8 μm). All of the 1D and 2D NMR spectra (^{1}H NMR, ^{13}C NMR, DEPT-135 NMR, ^{1}H–^{1}H COSY, HSQC, HMBC, and NOESY) were obtained on a Bruker Avance III 500 MHz spectrometer (Bruker BioSpin AG, Fällanden, Switzerland) or a Bruker Avance III HD 600 MHz spectrometer (Bruker Bio-Spin AG, Fällanden, Switzerland) using tetramethylsilane as an internal standard with chemical shifts reported in parts per million (ppm). Preparative high-performance liquid chromatography (HPLC) separations were carried out on Agilent 1200 HPLC system with an ODS column (50 cm × 34 mm, 50 μm; YMC Co., Ltd., Kyoto, Japan), BUCHI Pure C-815 Flash system (BÜCHI Labortechnik, Flawil, Switzerland) with a YMC Triart Prep C18 column (40 × 160 mm, 20 μm; YMC Co., Ltd., Kyoto, Japan), Hanbon NP7001C HPLC system (Hanbon Sci. & Tech, Jiangsu, China) with an Acchrom XCharge C18 column (20 × 250 mm, 5 μm), and a TBE-300B high-speed counter-current chromatography equipped with a Model TBP-1002 constant-flow pump and a Model TBD-2000UV detector (Tauto Biotech Co. Ltd, Shanghai, China). Semi-preparative HPLC purifications were carried out on an Agilent 1100 HPLC system with a VWD detector using an Agilent Eclipse XDB-C18 column (9.4 × 250 mm, 5 μm; Agilent Technologies, Palo Alto, CA, USA), or a Waters XSelect CSH C18 column (10 × 250 mm, 5 μm; Waters, Milford, MA, USA) for acidic mobile phase, and a Phenomenex Gemini C18 column (10 × 250 mm, 5 μm; Phenomenex, Torrance, CA, USA), or a Waters Xbridge Prep C18 column (10 × 250 mm, 5 μm; Waters, Milford, MA, USA) for alkaline mobile phase. Column chromatography (CC) was carried out on silica gel (200–300 mesh; Qingdao Marine Chemical, Inc., Qingdao, China), MCI gel (75–100 μm, Mitsubishi Chemical Co., Ltd., Japan), and macroporous resin D101 (Shanghai Sinopharm Chemical Reagent Co. Ltd., Shanghai, China). And preparative thin layer chromatography (TLC) was performed on PLC silica gel 60 F$_{254}$ plates (Merk Chemicals Co. Ltd., Shanghai, China).

The organic solvents for sample extraction, column chromatography, preparative HPLC, and preparative TLC were of analytical grade and supplied by Shanghai Sinopharm Chemical Reagent Co. Ltd. (Shanghai, China). Acetonitrile (MeCN; Shanghai Sinopharm Chemical Reagent Co. Ltd., Shanghai,

China), diethylamine (DEA; TCI, Tokyo, Japan), and formic acid (FA; Shanghai Aladdin Bio-Chem Technology Co. Ltd, Shanghai, China) applied in semi-preparative HPLC were of HPLC-grade, and ammonium acetate (NH$_4$OAc; ≥98%) was purchased from Sigma-Aldrich (St. Louis, MO, US). And the ultra-pure water was prepared by a Millipore Alpha-Q water purification system (Millipore, Bedford, USA).

Plant material

The dried lateral roots of *Aconitum carmichaelii* Debx. were purchased from Jiangyou, Sichuan province, China, in January 2019 and identified by Prof. De-an Guo. A voucher specimen was deposited at the National Engineering Laboratory for Traditional Chinese Medicine Standardization Technology, Shanghai Institute of Materia Medica, Chinese Academy of Sciences, Shanghai, China.

Extraction and isolation

The powdered dried lateral roots of *Aconitum carmichaelii* Debx. (10.0 kg) were extracted by heating at reflux with 75% ethanol (EtOH) for three times. After filtration, the extracting solvents were combined and evaporated under reduced pressure using a rotary evaporation equipment (Buchi, Switzerland) at the temperature of 40 °C. Subsequently, the obtained extracts (1.27 kg) were dissolved in distilled water, and successively applied for liquid–liquid partition using petroleum ether (PET; 60–90 °C), dichloromethane (CH$_2$Cl$_2$), ethyl acetate (EtOAc), and *n*-butanol (BuOH) saturated with water, and then evaporated under reduced pressure to obtain 38.49 g of the PET extracts, 76.71 g of the CH$_2$Cl$_2$ extracts, 7.66 g of the EtOAc extracts, and 151.28 g of the BuOH extracts. Integration of various chromatographic separation methods were carried out for further isolation and purification of DAs.

The PET extracts were separated on a silica gel column eluted with a gradient of PET–acetone containing 1% DEA (50 : 1–1 : 4, v/v) to afford 14 fractions (PET-Fr.1 to Fr.14). Among them, Fr.4 was separated using silica gel column with a gradient elution of cyclohexane–acetone containing 1% DEA (30 : 1–6 : 1), and then preparative TLC (*n*-hexane–EtOAc–DEA, 5 : 2 : 1, v/v) to give compound **33** (31 mg). Fr.5 and Fr.7 were directly purified by semi-preparative HPLC (55% MeCN–10 mM NH$_4$OAc containing H$_2$O, and 74% MeCN–5 mM NH$_4$OAc containing H$_2$O), and basified with aqueous saturated sodium bicarbonate to obtain compound **21** (2 mg) and **24** (4 mg), respectively. And preparative HPLC with a gradient of MeCN–5 mM NH$_4$OAc containing H$_2$O was applied to separate Fr.12, followed by semi-preparative HPLC (52% MeCN–5 mM NH$_4$OAc containing H$_2$O) and alkaline treatment to yield compound **22** (5 mg).

For CH$_2$Cl$_2$ extracts, an MCI gel column (500 g) was applied to obtain 14 fractions (Fr.1–Fr.14) with a gradient elution of 5–95% EtOH containing 0.5% ammonium hydroxide. Fr.2 (4.41 g) and Fr.11 (3.03 g) were subsequently loaded onto a Triart Prep C18 column on Flash system with the gradient elution of MeCN–H$_2$O (containing 0.015% DEA) to obtain Fr.2-1 to Fr.2-9, and Fr.11-1 to Fr.11-7, respectively. Semi-preparative HPLC (37% MeCN–0.015% DEA containing H$_2$O, and 33% MeCN–

0.015% DEA containing H$_2$O) was further applied in purification of Fr.2-5 (113.9 mg) and Fr.2-6 (39.8 mg) to obtain compound **10** (19 mg) and compound **9** (7 mg), respectively. Fr.11-6 (384.6 mg) was separated on Flash system using an ODS column and MeCN–0.1% FA containing H$_2$O as mobile phase, followed by preparative TLC (*n*-hexane–EtOAc–DEA, 5 : 2 : 1, v/v) to yield compound **28** (15 mg). And Fr.11-7 was purified by semi-preparative HPLC (67% MeCN–0.015% DEA containing H$_2$O) to give compound **2** (3 mg). Other fractions including fraction 3 (2.77 g), 6 (5.72 g), 10 (5.55 g), 13 (5.97 g), and 14 (8.39 g) were all separated on an ODS column on MHPLC system with a gradient elution of MeCN–0.1% FA containing H$_2$O to obtain Fr.3-1 to Fr.3-8, Fr.6-1 to Fr.6-11, Fr.10-1 to Fr.10-13, Fr.13-1 to Fr.13-7, and Fr.14-1 to Fr.14-9, respectively. And semi-preparative HPLC was further applied to obtain compound **4** (2 mg), **11** (77 mg), **29** (2 mg), **30** (14 mg), **32** (5 mg), **36** (5 mg), and **37** (17 mg) from the main subfractions of Fr.6, compound **5** (19 mg), **8** (14 mg), **12** (5 mg), **14a** (9 mg), **15** (47 mg), **16** (35 mg), **27** (20 mg), and **31** (21 mg) from subfractions of Fr.10, compound **20** (3 mg) and **26** (9 mg) from Fr.13, and compound **17** (3 mg), **18** (2 mg), **19** (15 mg), and **34** (2 mg) from Fr.14.

Besides, the BuOH extracts were chromatographed over a macroporous resin D101 column (1.5 kg) eluted with H$_2$O–EtOH (50 : 1 to 3 : 5) gradient system to give five fractions (Fr.1–Fr.5). Then an MCI column was applied to separate Fr.2 into 13 fractions (Fr.2-1 to Fr.2-13), among which Fr.2-8 was purified by semi-preparative HPLC (30% MeCN–0.015% DEA containing H$_2$O) to obtain compound **13** (25 mg), Fr.2-9, Fr.2-13 and Fr.2-12 were all successively separated by preparative HPLC (5–8% MeCN–0.1% FA containing H$_2$O), and semi-preparative HPLC (5% MeCN–0.1% FA containing H$_2$O, 7% MeCN–0.1% FA containing H$_2$O, and 40% MeCN–0.015% DEA containing H$_2$O) to afford compound **3** (7 mg), **7** (8 mg), **6** (68 mg), and **1** (12 mg), respectively.

In addition, HSCCC equipment was applied for rapid preparation of the major DAs in *Aconitum carmichaelii* Debx. As reported previously,[57] CH$_2$Cl$_2$–EtOAc–MeOH–0.3% HCl containing H$_2$O (2.75 : 1 : 1.5 : 2) and CH$_2$Cl$_2$–BuOH–MeOH–0.4% HCl containing H$_2$O were adopted as the solvent systems for separation of *Aconitum carmichaelii* Debx. and its processed products, respectively. And then preparative TLC was further used for purification of compound **23** (2 mg) and compound **35** (5 mg).

Hetisane-15β-*O*-β-D-glucoside (1). White, amorphous powder; $[\alpha]_D^{20}$ +14.8 (*c* = 0.1, CHCl$_3$); IR (Diamond ATR) ν_{max}: 3347, 2962, 2946, 2917, 2890, 2862, 1652, 1463, 1439, 1376, 1316, 1258, 1203, 1152, 1106, 1080, 1037, 1005, 990, 941, 885, 854 cm^{-1}; HR-ESI-MS (positive) at *m/z* 460.2702 [M + H]$^+$ (calcd for C$_{26}$H$_{38}$NO$_6$, 460.2699); ^{1}H (500 MHz, DMSO-d$_6$) and ^{13}C NMR (125 MHz, DMSO-d$_6$) data see Table 1.

6-Demethoxyhypaconine (14). White, amorphous powder; IR (Diamond ATR) ν_{max}: 3378, 2924, 1647, 1456, 1351, 1199, 1110, 1091, 732 cm^{-1}; HR-ESI-MS (positive) at *m/z* 440.2632 [M + H]$^+$ (calcd for C$_{23}$H$_{38}$NO$_7$, 440.2648); ^{1}H (600 MHz, CDCl$_3$) and ^{13}C NMR (150 MHz, CDCl$_3$) data see Table 2.

Carmichaeline K (17). White, amorphous powder; $[\alpha]_D^{20}$ −9.5 (*c* = 0.1, CHCl$_3$); IR (Diamond ATR) ν_{max}: 3416, 2924, 2819, 1716,

1602, 1584, 1492, 1451, 1367, 1317, 1277, 1197, 1164, 1093, 1052, 1034, 1004, 976, 917, 823, 714, 690 cm^{-1}; HR-ESI-MS (positive) at m/z 542.3129 $[M + H]^+$ (calcd for $C_{31}H_{44}NO_7$, 542.3118); ^1H (600 MHz, CDCl$_3$) and ^{13}C NMR (150 MHz, CDCl$_3$) data see Table 2.

8-*O*-Ethyl-benzoyldeoxyaconine (25). White, amorphous powder; $[\alpha]_D^{20}$ −3.7 ($c = 0.1$, CHCl$_3$); IR (Diamond ATR) ν_{max}: 3480, 2923, 2851, 1721, 1602, 1452, 1393, 1279, 1099, 981, 712 cm^{-1}; HR-ESI-MS (positive) at m/z 616.3509 $[M + H]^+$ (calcd for $C_{34}H_{50}NO_9$, 616.3486); ^1H (500 MHz, CDCl$_3$) and ^{13}C NMR (125 MHz, CDCl$_3$) data see Table 2.

8-*O*-Ethyl-benzoylhypaconine (26). White, amorphous powder; $[\alpha]_D^{20}$ −14.0 ($c = 0.1$, CHCl$_3$); IR (Diamond ATR) ν_{max}: 3416, 2924, 2819, 1716, 1602, 1583, 1492, 1451, 1367, 1317, 1277, 1197, 1164, 1093, 1052, 1034, 1004, 976, 917, 823, 714, 690 cm^{-1}; HR-ESI-MS (positive) at m/z 602.3336 $[M + H]^+$ (calcd for $C_{33}H_{48}NO_9$, 602.3329); ^1H (600 MHz, CDCl$_3$) and ^{13}C NMR (150 MHz, CDCl$_3$) data see Table S1.†

3-Deoxypyromesaconine (37). White, amorphous powder; $[\alpha]_D^{20}$ −116.2 ($c = 0.1$, CHCl$_3$); IR (Diamond ATR) ν_{max}: 3396, 2920, 2868, 2816, 2774, 1705, 1452, 1306, 1202, 1161, 1098, 989, 950, 897, 867, 831, 769 cm^{-1}; HR-ESI-MS (positive) at m/z 452.2636 $[M + H]^+$ (calcd for $C_{24}H_{38}NO_7$, 616.2648); ^1H (600 MHz, CDCl$_3$) and ^{13}C NMR (150 MHz, CDCl$_3$) data see Table S2.†

Cell culture and cell viability assays

Human lung cancer cell lines A549, H460 and human bronchial epithelial cell line HBE from the American Type Culture Collection (Manassas, VA34) were maintained in Dulbecco's modified Eagle's medium (Invitrogen, Grand Island, NY) supplemented with 100 units per μL penicillin, 100 μg mL^{-1} streptomycin and 10% fetal bovine serum at 37 °C in a 5% CO$_2$ incubator. Cells were seeded in 96-well plates at a concentration of 5×10^3 cells per well with complete culture medium and allowed to adhere to the plate overnight. Cell proliferation assays were performed using the MTT Cell Proliferation Kit (BSD Applied Science, Wuhan, China) according to the manufacturer's instructions. Each combination of cell line and drug concentration was set up in five replicates and repeated at least three times. Data were visualized using GraphPad Prism v.8.01 and IC$_{50}$ curves were fitted using a non-linear regression model with a sigmoidal dose response characteristic.

Network pharmacology analysis

All of the isolated DAs in this study were used to explore the "compound-target-pathway" network of DAs. Firstly, their chemical structures were converted into SMILES formats, and uploaded onto metaTarFisher (https://metatarget.scbdd.com/) search server for prediction of compound-associated targets. MetaTarFisher can be applied to obtain the possible targets of a compound based on its comprehensive information by integrating more than 10 widespread target fishing tools, including SwissTargetPrediction,[58] Similarity ensemble approach (SEA),[59] Polypharmacology Browser,[60,61] PASSonline,[62] TargetHunter,[63] HitPickV2,[64] TargetNet,[65] DNNTargetPridict, SimRanking,

ChemMapper,[66] and ChEMBL.[67] Meanwhile, genes associated with non-small-cell lung carcinoma were also explored using DisGeNET (https://www.disgenet.org/) platform. Intersection of the compound-associated targets and disease-associated targets were obtained, and Uniprot ID of these obtained targets were further transformed into preferred name (gene symbol) by ID mapping in STRING[68] database (https://string-db.org/) for the convenience of following gene enrichment analysis. And protein–protein interaction (PPI) analysis was also conducted using STRING database, choosing the parameters of organisms as *Homo sapiens*, and others default (medium confidence 0.400). Moreover, GO/KEGG enrichment analysis was performed on MetaScape[69] platform (https://metascape.org/) to interpret the possible molecular functions and pathways of these target genes, which was depicted by a bubble graph drawn in imageGP platform (http://www.ehbio.com/ImageGP/). At last, "compound-target-pathway" network was constructed using Cytoscape v3.8.2 software[70] to demonstrate the bioactive mechanisms of DAs, which may provide possible explanations to their anti-tumor activities, rendering a theoretical reference for future mechanism research.

Conclusions

A total of thirty-seven structurally diverse DAs were obtained from the lateral roots of *Aconitum carmichaelii* Debx., including three new natural compounds, one new DA derivative. Among them, compound **1** represented the first example of C$_{20}$-DA glucoside. The structures of all the isolated DAs were identified by a combination of HR-ESI-MS and NMR spectra, and their anti-tumor activities were systematically evaluated against human non-small-cell lung cancer cell lines A549 and H460 for discussion of their structure–activity relationships. Results showed that all the C$_{19}$-DAs exhibited moderate inhibitory activities with IC$_{50}$ values in the range of 7.97–28.42 μM, and positions C-8, C-10, C-14 and nitrogen atom in the C$_{19}$ skeleton were reckoned as the active sites, which may affect their anti-tumor activities. In addition, all of the isolated DAs were applied for network pharmacology analysis to interpret the possible mechanisms of DAs in treating cancer, laying the theoretical foundations for future research.

Author contributions

Conflicts of interest

There are no conflicts of interest to declare.

Acknowledgements

References

1 D. J. Newman and G. M. Cragg, *J. Nat. Prod.*, 2020, **83**, 770–803.

2 C. L. Yao, J. Q. Zhang, J. Y. Li, W. L. Wei, S. F. Wu and D. A. Guo, *Nat. Prod. Rep.*, 2021, DOI: 10.1039/d0np00057d.

3 W. J. Slichenmyer, E. K. Rowinsky, R. C. Donehower and S. H. Kaufmann, *J. Natl. Cancer Inst.*, 1993, **85**, 271–291.

4 F. P. Wang, Q. H. Chen and X. Y. Liu, *Nat. Prod. Rep.*, 2010, **27**, 529–570.

5 X. X. Liu, X. X. Jian, X. F. Cai, R. B. Chao, Q. H. Chen, D. L. Chen, X. L. Wang and F. P. Wang, *Chem. Pharm. Bull.*, 2012, **60**, 144–149.

6 L. Xiong, C. Peng, X. F. Xie, L. Guo, C. J. He, Z. Geng, F. Wan, O. Dai and Q. M. Zhou, *Molecules*, 2012, **17**, 9939–9946.

7 Y. P. Fan, Y. D. Jiang, J. J. Liu, Y. X. Kang, R. Q. Li and J. Y. Wang, *Bioorg. Med. Chem. Lett.*, 2016, **26**, 380–387.

8 F. Gao, Y. Y. Li, D. Wang, X. Huang and Q. Liu, *Molecules*, 2012, **17**, 5187–5194.

9 M. Y. Ren, Q. T. Yu, C. Y. Shi and J. B. Luo, *Molecules*, 2017, **22**, 267.

10 K. Wada and H. Yamashita, *Molecules*, 2019, **24**, 2317.

11 G. H. Zhou, L. Y. Tang, X. D. Zhou, T. Wang, Z. Z. Kou and Z. J. Wang, *J. Ethnopharmacol.*, 2015, **160**, 173–193.

12 S. Liu, F. Li, Y. Li, W. Li, J. Xu and H. Du, *J. Ethnopharmacol.*, 2017, **207**, 237–250.

13 M. Murayama, *Jpn. Pat.*, JP06016553A, 1994.

14 M. Murayama, *Jpn. Pat.*, JP07112971A, 1995.

15 L. V. Beshitaishvili and M. N. Sultankhodzhaev, *Chem. Nat. Compd.*, 1992, **28**, 206–208.

16 A. G. González, G. de La Fuente, M. Reina and R. D. Timón, *Phytochemistry*, 1986, **25**, 1971–1973.

17 X. X. Zong, X. J. Yan, J. L. Wu, Z. Q. Liu, H. Zhou, N. Li and L. Liu, *J. Nat. Prod.*, 2019, **82**, 980–989.

18 D. Csupor, P. Forgo, K. Csedo and J. Hohmann, *Helv. Chim. Acta*, 2006, **89**, 2981–2986.

19 T. Kiss, P. Orvos, S. Bánsághi, P. Forgo, N. Jedlinszki, L. Tálosi, J. Hohmann and D. Csupor, *Fitoterapia*, 2013, **90**, 85–93.

20 J. G. Díaz, J. G. Ruiz and G. de La Fuente, *J. Nat. Prod.*, 2000, **63**, 1136–1139.

21 Y. Liang, J. L. Wu, X. Li, M. Q. Guo, E. L. H. Leung, H. Zhou, L. Liu and N. Li, *Tetrahedron Lett.*, 2016, **57**, 5881–5884.

22 A. Ulubelen, *J. Nat. Prod.*, 1996, **59**, 360–366.

23 P. Forgo, B. Borcsa, D. Csupor, L. Fodor, R. Berkecz, V. A. Molnar and J. Hohmann, *Planta Med.*, 2011, **77**, 368–373.

24 Q. Li, S. D. Sun, M. Y. Wang, C. F. Li, D. Yuan and H. Z. Fu, *J. Chin. Pharm. Sci.*, 2018, **27**, 855–863.

25 W. Y. Liu, D. He, D. K. Zhao, Y. P. Chen and Y. Shen, *J. Asian Nat. Prod. Res.*, 2019, **21**, 9–16.

26 F. Zhang, S. L. Peng, X. Liao, K. B. Yu and L. S. Ding, *Planta Med.*, 2005, **71**, 1073–1076.

27 W. Wei, X. W. Li, H. Y. Zhou, R. J. Yang, X. L. Shi, J. Shan, L. Meng and Y. R. Jin, *J. Jilin Univ., Sci. Ed.*, 2010, **48**, 127–132.

28 C. Konno, M. Shirasaka and H. Hikino, *J. Nat. Prod.*, 2004, **45**, 128–133.

29 F. P. Wang and S. W. Pelletier, *J. Nat. Prod.*, 2004, **50**, 55–62.

30 W. Wei, X. W. Li, Y. R. Jie, X. L. Shi and H. F. Sun, *Chin. J. Magn. Reson.*, 2010, **27**, 238–248.

31 H. C. Wang and A. N. Lao, *Heterocycles*, 1988, **27**, 1615–1621.

32 Z. T. Zhang, L. Wang, Q. F. Chen, Q. H. Chen, D. L. Chen, X. Y. Liu and F. P. Wang, *Tetrahedron*, 2013, **69**, 5859–5866.

33 L. M. Gao, H. Y. Yan, Y. Q. He and X. M. Wei, *J. Integr. Plant Biol.*, 2006, **48**, 364–369.

34 H. L. Yu and S. S. Jia, *Acta Pharmacol. Sin.*, 2000, **35**, 232–234.

35 H. Hikino, Y. Kuroiwa and C. Konno, *J. Nat. Prod.*, 2004, **46**, 178–182.

36 H. M. Liu and A. Katz, *J. Nat. Prod.*, 1996, **59**, 135–138.

37 J. M. Yue, X. Jun and Y. Z. Chen, *Phytochemistry*, 1994, **35**, 829–831.

38 S. H. Shim, J. S. Kim, S. S. Kang, K. H. Son and K. Bae, *Arch. Pharmacal Res.*, 2003, **26**, 709–715.

39 S. W. Pelletier and Z. Djarmati, *J. Am. Chem. Soc.*, 1976, **98**, 2626–2636.

40 T. P. Yin, Y. Shu, H. Zhou, L. Cai and Z. T. Ding, *Fitoterapia*, 2019, **135**, 1–4.

41 F. P. Wang, and X. T. Liang, in *Alkaloids Chem. Biol.*, ed. G. A. Cordell, Academic Press, Pittsburgh, 2002, vol. 59, pp. 1–280.

42 T. Tanaka, T. Nakashima, T. Ueda, K. Tomii and I. Kouno, *Chem. Pharm. Bull.*, 2007, **55**, 899–901.

43 X. H. Meng, Q. L. Guo, C. G. Zhu and J. G. Shi, *Chin. Chem. Lett.*, 2017, **28**, 1705–1710.

44 Q. Guo, H. Xia, X. Meng, G. Shi, C. Xu, C. Zhu, T. Zhang and J. Shi, *Acta Pharm. Sin. B*, 2018, **8**, 409–419.

45 F. P. Wang, and Q. H. Chen, in *Alkaloids Chem. Biol.*, ed. G. A. Cordell, Academic Press, Pittsburgh, 2010, vol. 69, pp. 1–577.

46 F. P. Wang, D. L. Chen, H. Y. Deng, Q. H. Chen, X. Y. Liu and X. X. Jian, *Tetrahedron*, 2014, **70**, 2582–2590.

47 B. Jiang, S. Lin, C. Zhu, S. Wang, Y. Wang, M. Chen, J. Zhang, J. Hu, N. Chen, Y. Yang and J. Shi, *J. Nat. Prod.*, 2012, **75**, 1145–1159.

48 B. Y. Jiang, S. Lin, C. G. Zhu, S. J. Wang, Y. N. Wang, M. H. Chen, J. J. Zhang, J. F. Hu, N. H. Chen, Y. C. Yang and J. G. Shi, *J. Nat. Prod.*, 2013, **76**, 2008.

49 I. Vivanco and C. L. Sawyers, *Nat. Rev. Cancer*, 2002, **2**, 489–501.

50 S. Revathidevi and A. K. Munirajan, *Semin. Cancer Biol.*, 2019, **59**, 80–91.

51 I. Pal and M. Mandal, *Acta Pharmacol. Sin.*, 2012, **33**, 1441–1458.

52 S. Lee and K. Margolin, *Cancers*, 2011, **3**, 3856–3893.

53 M. B. Atkins, *Semin. Oncol.*, 2002, **29**, 12–17.

54 M. Cargnello and P. P. Roux, *Microbiol. Mol. Biol. Rev.*, 2011, **75**, 50–83.

55 Y. J. Guo, W. W. Pan, S. B. Liu, Z. F. Shen, Y. Xu and L. L. Hu, *Exp. Ther. Med.*, 2020, **19**, 1997–2007.

56 C. Lin, D. R. Crawford, S. Lin, J. Hwang, A. Sebuyira, R. Meng, J. E. Westfall, H. Y. Tang, S. Lin, P. Y. Yu, P. J. Davis and H. Y. Lin, *Carcinogenesis*, 2011, **32**, 19–26.

57 Q. B. Han, W. L. Tang, C. X. Dong, H. X. Xu and Z. H. Jiang, *J. Sep. Sci.*, 2013, **36**, 1304–1310.

58 D. Gfeller, A. Grosdidier, M. Wirth, A. Daina, O. Michielin and V. Zoete, *Nucleic Acids Res.*, 2014, **42**, W32–W38.

59 M. J. Keiser, B. L. Roth, B. N. Armbruster, P. Ernsberger, J. J. Irwin and B. K. Shoichet, *Nat. Biotechnol.*, 2007, **25**, 197–206.

60 M. Awale and J. L. Reymond, *J. Cheminf.*, 2017, **9**, 11.

61 M. Awale and J. L. Reymond, *J. Chem. Inf. Model.*, 2019, **59**, 10–17.

62 P. V. Pogodin, A. A. Lagunin, D. A. Filimonov and V. V. Poroikov, *SAR QSAR Environ. Res.*, 2015, **26**, 783–793.

63 L. R. Wang, C. Ma, P. Wipf, H. B. Liu, W. W. Su and X. Q. Xie, *AAPS J.*, 2013, **15**, 395–406.

64 S. Hamad, G. Adornetto, J. J. Naveja, A. Chavan Ravindranath, J. Raffler and M. Campillos, *Bioinformatics*, 2019, **35**, 1239–1240.

65 Z. J. Yao, J. Dong, Y. J. Che, M. F. Zhu, M. Wen, N. N. Wang, S. Wang, A. P. Lu and D. S. Cao, *J. Comput.-Aided Mol. Des.*, 2016, **30**, 413–424.

66 J. Y. Gong, C. Q. Cai, X. F. Liu, X. Ku, H. L. Jiang, D. Q. Gao and H. L. Li, *Bioinformatics*, 2013, **29**, 1827–1829.

67 A. Gaulton, A. Hersey, M. Nowotka, A. P. Bento, J. Chambers, D. Mendez, P. Mutowo, F. Atkinson, L. J. Bellis, E. Cibrian-Uhalte, M. Davies, N. Dedman, A. Karlsson, M. P. Magarinos, J. P. Overington, G. Papadatos, I. Smit and A. R. Leach, *Nucleic Acids Res.*, 2017, **45**, D945–D954.

68 D. Szklarczyk, A. L. Gable, D. Lyon, A. Junge, S. Wyder, J. Huerta-Cepas, M. Simonovic, N. T. Doncheva, J. H. Morris, P. Bork, L. J. Jensen and C. V. Mering, *Nucleic Acids Res.*, 2019, **47**, D607–D613.

69 Y. Zhou, B. Zhou, L. Pache, M. Chang, A. H. Khodabakhshi, O. Tanaseichuk, C. Benner and S. K. Chanda, *Nat. Commun.*, 2019, **10**, 1523.

70 P. Shannon, A. Markiel, O. Ozier, N. S. Baliga, J. T. Wang, D. Ramage, N. Amin, B. Schwikowski and T. Ideker, *Genome Res.*, 2003, **13**, 2498–2504.